Investigating the Productivity and Sustainability of Weathered Basement Aquifers in Tropical Africa Using Numerical Simulation and Global Sensitivity Analysis

Marco Bianchi[1] , **Alan M. MacDonald[2]** , **David M. J. Macdonald[3]** , **and Enoch B. Asare[4]**

[1]British Geological Survey, Keyworth, UK, [2]British Geological Survey, Edinburgh, UK, [3]British Geological Survey, Wallingford, UK, [4]Water Resources Commission, Accra, Ghana

Abstract Groundwater stored in weathered basement aquifers (WBAs) is a strategic water resource. In this study, we investigate the productivity of WBAs and sustainability of groundwater abstractions using a novel process-based stochastic modeling approach, which is applied to simulate abstractions in the Precambrian basement aquifer in Ghana. The statistical distribution of the generated synthetic yield data was found in very good agreement with observed yield data from the same Ghanaian aquifer. Further analysis provided robust insights regarding how different hydrogeological parameters of the WBA, and their interplay, control aquifer productivity and sustainability. Results indicate that 97% of the simulated abstractions could sustain the yield of a hand pump (6 L/min), approximately 30% could also sustain yields >60 L/min, while only 1% could sustain yields greater than 300 L/min. The model indicates that an aquifer transmissivity value of approximately 1.4 m²/day is required for a successful hand-pumped borehole, while a higher yielding source (60 L/min) requires a transmissivity value of at least 9.5 m²/day. A global sensitivity analysis of 13 model input parameters shows that the thickness of the regolith and the maximum hydraulic conductivity developed at the base of the saprolite are the critical factors controlling success and sustainability for low yielding hand-pumped boreholes. For higher yielding supplies, the net recharge, the depth to groundwater, and the aquifer extent become increasingly significant. Results from this work have important implications for the potential for increased development of groundwater from WBAs in tropical Africa.

1. Introduction

Crystalline (igneous and metamorphic) rocks underlie approximately 34% of Africa's land surface, where approximately half of the rural population live (MacDonald & Calow, 2009). Much of the rural population depend on groundwater from the weathered basement as their primary source of drinking water, abstracting groundwater mostly with shallow wells and boreholes equipped with hand pumps (WHO/UNICEF, 2020). As demand for a reliable source of fresh water rises, groundwater stored in basement aquifers is expected to become increasingly developed due to its widespread availability (Braune & Xu, 2010; MacDonald et al., 2012) and ability to buffer climatic variability (Calow et al., 2010; Cuthbert et al., 2019; Taylor et al., 2013). The predicted increase in abstraction is not only to address the lack of basic drinking water (WHO/UNICEF, 2020) but also for an increase in productive uses, mainly irrigation (Agrawal & Jain, 2019; Altchenko & Villholth, 2015), to help achieve the Sustainable Development Goals (SDG) (Velis et al., 2017). Increased abstraction from weathered basement aquifers (WBAs) is also driven by advances in water lifting technologies, particularly those powered by renewable energy resources (Chandel et al., 2015; Wazed et al., 2018), and increased use of reticulated systems to meet the SDG of safely managed water (Velis et al., 2017).

The average groundwater source yield (productivity) of WBAs in Africa is generally low (<60 L/min; MacDonald et al., 2012) due to typically low transmissivity and storativity values (Chilton & Foster, 1995; Howard et al., 1992; Ofterdinger et al., 2019; Taylor & Howard, 2000). However, yields from individual boreholes can vary substantially (Courtois et al., 2010; Jones, 1985; Macdonald & Edmunds, 2014; McFarlane et al., 1992), and hydrogeological conditions sustaining high-intensity abstractions are possible (Maurice et al., 2019). Hydrogeological investigations of WBAs in different parts of the world have shown that groundwater flow is commonly compartmentalized (Acworth, 1987; Dewandel et al., 2006; Howard et al., 1992;

Taylor & Howard, 2000; Wright, 1992). The main productive zone within these aquifers corresponds to the highly fractured rock at the base of the weathered portion of the profile (regolith); the fractures within the consolidated bedrock have declining influence on the productivity with depth (Ayraud et al., 2008; Collins et al., 2020; Guihéneuf et al., 2014; Maréchal et al., 2004). This complex vertical distribution of aquifer properties makes assessing productivity and sustainable management challenging because well yields do not simply depend on static hydrogeological properties (e.g., hydraulic conductivity, transmissivity, storage, and fracture frequency) but also on hydrodynamic factors (e.g., water table depth and recharge rate) and their complex interplay. Increased abstraction over time, for instance, can lead to dewatering of the most productive part of the aquifer, dramatically reducing well yields and limiting lateral flow (Guihéneuf et al., 2014; Perrin et al., 2011).

The previous considerations highlight some of the limitations of early attempts to find empirical relationships between indicators of well performance (i.e., yield and specific capacity) and environmental conditions (e.g., relief and regolith thickness) or well construction parameters (e.g., depth) in WBAs (Barker et al., 1992; Houston & Lewis, 1988; McFarlane et al., 1992). Furthermore, well performance data, particularly yield, are subject to a high degree of uncertainty, limiting the effectiveness of these relationships for well siting and productivity mapping (Chilton & Foster, 1995; Taylor & Howard, 2000). Recent studies addressed the issue of predicting the potential productivity of WBAs by focusing on upscaling and mapping of the hydrogeological properties with various approaches: geostatistical methods (Razack & Lasm, 2006); relationships between geophysical and hydrogeological properties (Chandra et al., 2008; Meju et al., 2001; Shishaye et al., 2019); multicriteria analysis using GIS (Lachassagne et al., 2001); large-scale fluctuations in hydraulic heads (Dewandel et al., 2017) in combination with satellite data (Dewandel et al., 2017; Macdonald & Edmunds, 2014); the integration of borehole data and geological mapping (Courtois et al., 2010; MacDonald et al., 2012); and probabilistic and machine learning models (Ahmed & Mansor, 2018).

Although previous approaches allow a quantitative estimation of the groundwater yield, they cannot take into account the transient nature of groundwater flow dynamics and in particular nonlinearity with depth. As a result, the hydrogeological processes that govern groundwater productivity and sustainability in WBAs are still not sufficiently characterized. In this study, we propose a physically based stochastic modeling approach to understand the interplay of the different climatic, geological, hydrogeological, and construction parameters influencing aquifer productivity. In particular, we design a numerical experiment to explore different combinations of input parameters and their effect on borehole performance data. A novel stochastic approach is developed for generating 1-D spatial distributions of hydrogeological properties, and numerical simulations of transient groundwater flow are conducted for calculating the evolution of sustainable yields over a multiyear period representing cycles of wet and dry seasons. The resulting synthetic borehole performance data, validated against a large data set from northern Ghana (Carrier et al., 2011), were considered for a global sensitivity analysis (Pianosi & Wagener, 2015) to explore relationships between different inputs and quantify the relative contribution of their variability on productivity and sustainability of the abstractions.

2. Conceptual Hydrogeological Model of a Generic WBA

The established hydrogeological conceptual model of the weathered profile of crystalline basement rocks in tropical Africa includes (from the ground surface with depth): a few meters of residual soil (RS) that often comprise ferralitic soils with laterite pisoliths; an upper saprolite (US) layer composed of mainly secondary clay minerals, with thickness ranging from a few to tens of meters; a lower saprolite (LS) layer, similar to the US in thickness but with a much higher proportion of primary minerals; and a fractured layer, up to tens of meters thick, referred to as the saprock (SR), transitioning with depth into the underlying unweathered basement rock (Acworth, 1981; Chilton & Foster, 1995; Dewandel et al., 2006; Jones, 1985). Each layer has a specific lithomineralogical composition and structure due to chemical and physical weathering of the crystalline rock (Fookes, 1997). The assemblage of the layers results in a composite aquifer with significant vertical variability in the hydrogeological properties (Figure 1).

The RS and the saprolite layers form a largely unconsolidated part of the profile, also known as the regolith. The RS can have high hydraulic conductivity (K), particularly if laterite has developed (Bonsor et al., 2014). The high fraction of secondary clay minerals in the US layer often results in low K values (10^{-7} to 10^{-9} m/s; Chilton & Foster, 1995; McFarlane et al., 1992), while porosity (n) generally is at its maximum here (≈ 0.3).
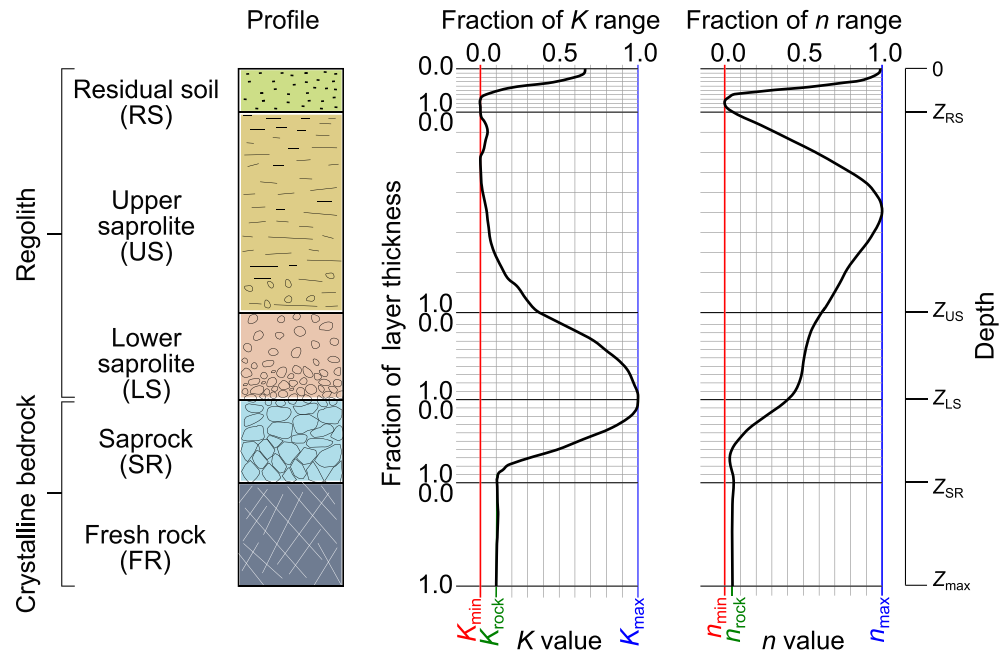
Figure 1. Conceptual model of physical heterogeneity in a weathered basement aquifer.

Consequentially, the US cannot sustain groundwater abstractions but does provide storage capacity. As the volumetric fraction of secondary clay minerals diminishes and the amount of mineral quartz and rock fragments increases toward the base of the saprolite layer, K gradually increases within the LS reaching a maximum value in the order of 10^{-4} to 10^{-5} m/s (Boisson et al., 2015; Edet & Okereke, 2005; McFarlane et al., 1992), corresponding with a basal brecciated zone at the interface between the LS and SR (Chilton & Foster, 1995). The presence of this relatively permeable and generally productive zone at the bottom of the regolith increases the composite transmissivity of the regolith. Dense horizontal fracturing in the SR maintains relatively high K values in this layer, especially within the few meters below the regolith, as indicated by flowmeter and packer tests data in African and Indian WBAs, which have a geometric mean of the order of 10^{-5} m/s (Dewandel et al., 2006; Maréchal et al., 2004). Fracturing and degree of weathering in the SR layer decreases with depth causing a reduction in K until values become representative of the matrix of fresh crystalline rock (FR). The bulk K of FR is low (10^{-7} to 10^{-9} m/s; Dewandel et al., 2006; Howard et al., 1992), although locally higher K values associated with tectonic fractures are not unusual at depths up to 200 m below ground level. These discrete productive zones can produce transmissivities with values typically in the order of a few m^2/day (Howard et al., 1992; Taylor & Howard, 2000) or higher (Maurice et al., 2019; Taylor et al., 2013).

Aquifer extents in weathered basement rocks can be highly variable, depending on the lateral continuity of weathered horizons and the presence of discharge areas within shallow valleys. Geophysical surveys used to site rural water supply boreholes Africa have shown weathering thickness to be highly variable even on a kilometer scale (Belle et al., 2019). Since groundwater flow is generally shallow (within the top 30 m or so) and K reduces significantly with depth, it is unusual for groundwater to flow for more than 1–5 km before intersecting a valley or discharge point. Even in more permeable WBAs in peninsular India, groundwater flow paths were found to be less than 5 km (Collins et al., 2020).

3. Methods

3.1. Generation of Representative Profiles of Hydraulic Conductivity and Porosity

Vertical 1-D distributions of hydrogeological parameters (K and n) were generated with an approach conceptually similar to multiple-point geostatistical methods (e.g., Mariethoz & Caers, 2014), which generate spatial distributions of a variable of interest, honoring the characteristic patterns and trends shown by a
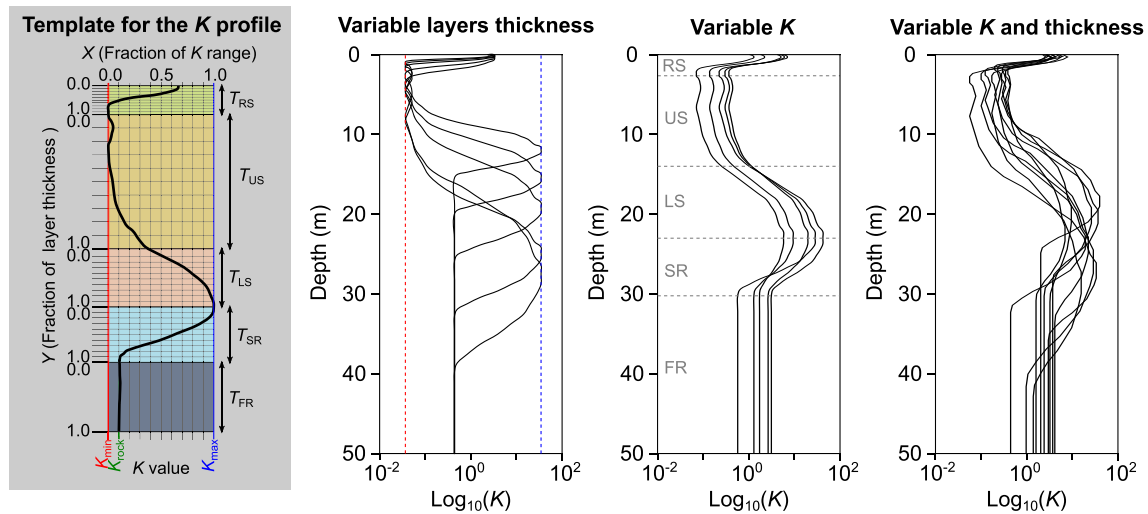
Figure 2. Generation of representative profiles of heterogeneity for a generic WBA.

so-called training image. The approach developed generates stochastic realizations of the vertical profiles of K and n for a synthetic WBA according to the trends in two template profiles (Figure 1), which are representative of the established conceptual model proposed by Chilton and Foster (1995). This conceptualization of the weathered profile was developed using data from African WBAs (Barker et al., 1992; Hazell et al., 1992; Wright, 1992) and was confirmed by subsequent hydrogeological investigations (e.g., Dewandel et al., 2006; Maréchal et al., 2004). The approach for generating different K profiles is illustrated in Figure 2. The five layers in the template vertical profile have thickness T_{RS} for the RS, T_{US} for the US layer, T_{LS} for LS layer, T_{SR} for the SR, and T_{FR} for the FR. For each layer of the regolith (RS + US + LS) and the SR, the conceptual K profile was discretized into points in the space xy. The coordinates x of these points are defined as fractions of the range in $\log_{10}(K)$ values in the profile. Accordingly, for each point:

$$x = \Delta K / [\log_{10}(K_{\min}) - \log_{10}(K_{\min})] \tag{1}$$

where $K_{\min}$ and $K_{\max}$ are the minimum and maximum K values, respectively, while ΔK is the increment in $\log_{10}(K)$ with respect to $K_{\min}$. Values for the coordinates y are defined as fractions of layer thickness. Therefore, for a generic layer i, $y = z/T_i$, where z is depth relative to the top boundary and T_i is the total thickness ($T_i = \sum z$).

The adopted conceptual model assumes smooth variability with depth in the conductivity and porosity profiles of a WBA (Figure 1). In particular, the minimum value of the K profile occurs near the boundary between the RS and the US, where there is the maximum concentration of secondary clay minerals. Experimental studies have shown that higher conductivity within the LS and SR layers is the result of the presence of a dense network of vertical and horizontal fissures, rather than the contribution of a single highly conductive fracture (e.g., Maréchal et al., 2004). Therefore, in the proposed model, this dense fracture network is assumed to behave as an equivalent porous medium (e.g., Long et al., 1982), and the contribution of the fractures to the total permeability of the aquifer and hence to groundwater flow is considered by the variability of the K profile with depth. Changes in fracture density and aperture in the different layers of the WBAs are reflected by the relatively smooth increment in K within the LS, the peak in K at the interface between LS and SR, and the equally smooth decline in K within the SR (Figure 1). This conceptualization will be further discussed together with other potential limitations of the proposed modeling approach. The hydraulic conductivity of the bottom layer (K_{FR}) is also assumed to represent the equivalent K (Renard & De Marsily, 1997) of the fractured FR, such as, for instance, the value estimated from a constant rate pumping test. Therefore, although individual fractures in the FR are not explicitly represented in the flow model, their contribution to the bulk transmissivity of this layer is still considered although the basement fractured aquifer is represented as an equivalent porous medium.
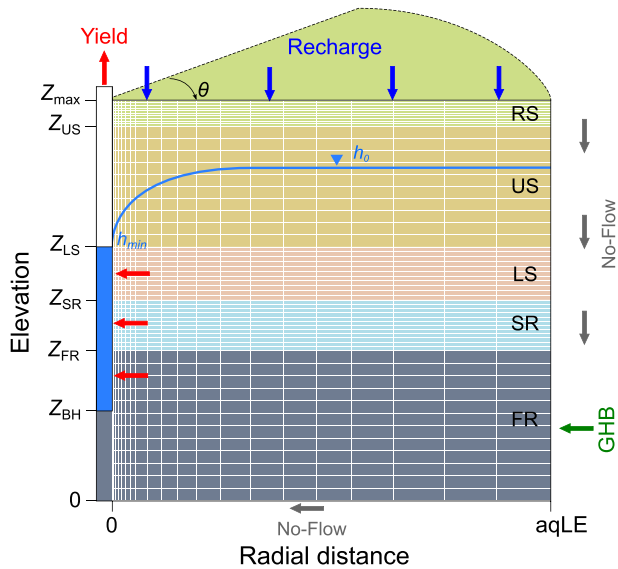
Figure 3. Numerical model setup. Parameter abbreviations are described in the main text and in Table 1.

Log-transformed K values were used for the generation of the K profiles, to reproduce the variations of orders of magnitude between different layers typically observed in WBAs (Bonsor et al., 2014). Effective porosity profiles were generated using the parameters n_{min}, n_{max}, and n_{rock} (Figure 1) with an approach analogous to the one described for K, but not log-transforming values given the generally low range of variability of this hydrogeological property in these geological media.

With the computed coordinates (x, y), a "K versus depth" profile is generated in two steps. First, given an array of x coordinates, K values for generic layer i are computed as follows:

$$\log_{10}(K) = \log_{10}(K_{min}) + x \cdot [\log_{10}(K_{max}) - \log_{10}(K_{min})] \quad (2)$$

Then, corresponding depth values Z are calculated as

$$Z = T_{i-1} + T_i \cdot y \quad (3)$$

where T_{i-1} is the thickness of the layer above. For the layer representing the RS, T_{i-1} is 0.

As shown in the illustrative examples presented in Figure 2, the proposed approach is very flexible, and it can produce a wide range of heterogeneity profiles that are consistent with the fundamental trends of conductivity and porosity of the template models. Moreover, the approach is suitable for stochastic generation when statistical distributions of the input parameters are provided.

3.2. Numerical Simulations of Groundwater Abstraction and Aquifer Productivity

An axisymmetric groundwater transient flow model was developed to simulate groundwater abstraction from a borehole located within the generated WBA profiles. Radial flow was simulated using a 2-D finite-difference Cartesian grid and the code MODFLOW-2005 (Harbaugh, 2005). Following the procedure proposed by Langevin (2008) for modeling axisymmetric flow using Cartesian grids, input parameters assigned to each grid block (i.e., hydraulic conductivity, specific storage, and recharge) were adjusted to account for increments in the flow area with radial distance (Langevin, 2008; Louwyck et al., 2014). With this approach, the radial domain is represented by a vertical cross section discretized with a rectangular grid extending to a distance equal to $aqLE$ laterally and to Z_{max} vertically (Figure 3). Grid spacing in the vertical direction considers 10 blocks for each layer of the WBA profile, while the width of the columns increases logarithmically away from the borehole located in the first column, which has a width equal to the borehole radius (a standard 6 in. = 152.4 mm diameter borehole is assumed). Grid block transmissivities for the model layers are calculated from the saturated thickness and the corresponding K values in the generated vertical profiles. The logarithmic weighting option was used to calculate the interblock conductances as in Langevin (2008). Assigned specific yield values correspond to the values in the generated n profiles.

The transient groundwater flow is simulated for a period of 5 years discretized into monthly stress periods and daily time steps. If a cell becomes "dry" and inactive (i.e., head drops below the bottom elevation) during a time step, it can be reactivated according to heads in the adjacent cells using the rewetting option in MODFLOW. A uniform hydraulic head equal to h_0 is assumed at the beginning of the simulation. Boundary conditions include a no-flow condition applied to the bottom of the domain and a specified flux condition representing aquifer recharge to the top. In the application considered in this study, a tropical climate with a discrete wet season of 4 months was simulated; accordingly, for each year of simulated time, a constant flux representing the net groundwater recharge is applied only for the four stress periods of the wet season. A no-flow boundary condition is applied to the cells representing the regolith and SR layers, located at a radial distance equal to $aqLE$, while a Cauchy condition (i.e., general head boundary [GHB]) is applied to corresponding cells in the fractured bedrock. With the latter conditions, we assume a finite extension for the weathered section of the WBA, while the fractured FR layer is infinite and can provide a source of water in the form of baseflow. The only sink in the domain is the abstraction borehole, which is simulated by

assigning a constant hydraulic head (h_{min}) and a very large K value to the cells located in the first column above elevation Z_{BH} (Figure 3). The borehole can partially penetrate the domain, but it is assumed to be open or to fully screen the saturated thickness. The borehole yield equivalent to the time-varying abstraction rate is calculated from the cell-by-cell water balance of the model, which is monitored every time step. These yields are controlled by the hydraulic gradient around the borehole, which is particularly steep and highly variable in the first few time steps of the simulation due to the sudden head drop from h_0 to h_{min} imposed at the borehole. Therefore, a warm-up period of 1 year was considered before starting to measure yields at the abstraction borehole.

The assigned head h_{min} in the borehole has a particular meaning for the purpose of this work. It is defined as follows:

$$\begin{cases} h_{min} = Z_{LS}, & \text{if } h_0 > Z_{LS} \\ h_{min} = Z_{SR}, & \text{if } Z_{SR} < h_0 < Z_{LS} \end{cases} \tag{4}$$

where Z_{LS} and Z_{SR} are the elevations of the top boundaries of the LS and SR, respectively (Figure 3). The rationale behind this definition is the typical location of the productive layer in WBAs crossing the interface between these two layers. Therefore, it is logical to define an optimal sustainable abstraction rate as the yield that, under pumping conditions, does not cause the water level in the abstraction borehole to fall below either the LS or the SR layer, depending on the depth of the static water table relative to these layers. This optimal rate, which is estimated for each time step of the numerical simulation, can also be regarded as the maximum allowable yield of the saprolite and SR layers, which is the primary objective of this work.

Groundwater flow modeling was also applied to estimate of the equivalent transmissivity (T_{eq}) of the generated WBA profiles. For this calculation, a modification of the boundary conditions shown in Figure 3 was necessary; the GHB boundary to the fractured bedrock at *aqLE* was extended to the regolith layer. This adjustment is equivalent to assuming an infinite extension for all the layers of the WBA. The model was also run for an extended simulation period until steady-state conditions were assumed. The equivalent transmissivity of the profile can be estimated using the Thiem equation in the form:

$$T_{eq} = \frac{Q}{2\pi(h_0 - h_{min})} \ln\left(\frac{aqLE}{r_w}\right) \tag{5}$$

where Q is the calculated abstraction rate at the borehole at the end of the simulation and r_w is the radius of the borehole.

3.3. Numerical Experiment Design and Generation of Synthetic Data Set of Borehole Performance

A numerical experiment was designed to generate a comprehensive synthetic data set of maximum allowable yields for the weathered Precambrian basement aquifer of northern Ghana. The objectives of this experiment were to test the reliability of the simulated outputs against actual borehole data and then use the generated data set of estimated yields to understand which parameters have greater control on groundwater productivity. Data presented in the comprehensive hydrogeological study by Carrier et al. (2011), which include statistical analysis of more than 7,000 reliable borehole technical data and results from pumping tests, integrated with hydrogeological data from published studies considering this region (Acheampong & Hess, 1998; Dapaah-Siakwan & Gyau-Boakye, 2000; Forkuor et al., 2013), as well as other sub-Saharan African countries (Chilton & Foster, 1995; Howard et al., 1992), were used for the design of the numerical experiment.

A set of Latin hypercube (LH) random samples ($N = 50,000$) were generated for 13 model input parameters. The list of parameters (Table 1) includes geological and hydrogeological parameters for the definition of the K and n profiles, parameters describing hydraulic conditions, stresses, and the lateral extension of the WBA, as well as the depth of the borehole. Since the regolith layers and the SR are the product of weathering processes acting on the fresh basement rock, their thicknesses depend on a complex interplay of local and regional factors such as geology, relief, tectonic processes, latitude, and past and present climate (Acworth, 1987; Collins et al., 2020; Dewandel et al., 2006; Taylor & Howard, 2000; Wright, 1992). However, because the

Table 1
Model Input Parameters

Variable	Description
RT	Total thickness of the regolith
RST	Thickness of the residual soil
LSf	Fraction of RT for the lower saprolite
SRf	Thickness ratio between saprock and lower saprolite
wtD	Water table depth
K_{min}	Minimum value in the K profile (see Figure 1)
K_{max}	Maximum value in the K profile (see Figure 1)
K_{rock}	Equivalent K of the bedrock (see Figure 1)
$minn$	Minimum effective porosity (see Figure 1)
$maxn$	Maximum effective porosity (see Figure 1)
bhD	Maxim borehole depth
$rech$	Total annual recharge rate
$aqLE$	Aquifer lateral extent (see Figure 3)

duration of the weathering acting on a certain profile is also a primary factor (Wright, 1992), the thicknesses of the different constitutive layers are not independent. To account for this interdependency, and to generate profiles with a higher degree of realism, the thicknesses of the saprolite and SR layers were defined as a function of the total thickness of the regolith (RT), the thickness of the RS (T_{RS}), and two factors. These two represent the relative thickness of the US with respect to total saprolite thickness (LSf) and the ratio between the thicknesses of the US and SR layer (SRf). In particular: The total thickness of the saprolite ($T_S = T_{US} + T_{LS}$; see Figure 1) was defined by the difference between RT and T_{RS}; the thickness of the LS was defined as the product between T_S and LSf ($T_{LS} = T_S \cdot LSf$); while the thickness of the SR was defined as the product between T_{LS} and SRf ($T_{SR} = T_{LS} \cdot RSf$). All the other parameters in Table 1 are otherwise independent.

For all samples, the maximum vertical extension of the modeled cross section was set equal to 100 m, which is consistent with hydrogeological observations regarding the likely maximum depth for active groundwater circulation in WBAs in Africa (Boisson et al., 2015; Maréchal et al., 2004) and borehole depth data (Carrier et al., 2011; Chilton & Foster, 1995; Courtois et al., 2010). Therefore, the thickness of the FR model layer is calculated as the difference between this maximum vertical extension and the sum of the thicknesses of the other layers. The initial groundwater level (h_0) was also calculated from the difference between the maximum vertical extension and the water table depth (wtD).

LH samples representing dry or technically negative boreholes were not considered for numerical simulation of groundwater abstraction. These samples presented at least one of following conditions: (1) h_0 is less than 2 m above the bottom of the borehole; (2) the difference between h_0 and the level imposed at the borehole during the numerical simulation (h_{min}; see Equation 4) is less than 1 m; and (3) h_0 is below the elevation of the top of the saprolite layer (Z_{SR} in Figure 1). The first and second conditions were imposed to account for the standard values for the minimum operational head gradient and minimum water elevation for submersible pumps. The third condition was applied because groundwater productivity of the lower portion of the saprolite layer and the unweathered crystalline rock is controlled by the frequency and the geometry of the flowing fractures intercepting the borehole. Taking into account these factors would have required a different modeling approach for simulating flow in fracture media (e.g., Maréchal et al., 2004), while in this work, we focused on the productivity of the weathered porous layers forming a WBA.

The statistical distributions assigned to the 13 input parameters for the numerical experiment are presented in Table 2. A uniform distribution was assumed for the parameters, except for K_{max} and K_{rock}, for which a log-normal distribution was assumed. Given the lack of data regarding the variability of K in the weathered Precambrian basement aquifer, the mean and the variance values of these log-normal distributions were computed by means of a series of calibrations runs with the objective of matching the calculated transmissivity of the synthetic profiles (T_{eq}, Equation 5) to the available reference data from pumping tests presented by Carrier et al. (2011). The distributions of values considered for K_{max} and K_{rock} determined with this calibration exercise are also comparable with typical values of the regolith and the fractured crystalline bedrock layers (Boisson et al., 2015; Howard et al., 1992; Maréchal et al., 2004; Taylor & Howard, 2000).

For each set of input parameters, a corresponding time series of maximum allowable yields over a period of 4 years was calculated with the numerical model. In order to validate this synthetic data set, we considered the average values for each time series, and the cumulative distribution and descriptive statistics of these average values were compared to those of actual yield values measured in 576 boreholes in the Precambrian aquifer in Ghana (Carrier et al., 2011). Note, these boreholes were located primarily by proximity to water-stressed rural communities rather than as a result of hydrogeological investigation. The average maximum allowable yields provide general information regarding the productivity associated with the WBA profiles. However, the variability of the simulated maximum yields over the simulated period can explain the sustainability of these abstractions and their relationships with respect to the different

Table 2
Statistical Distributions of the Input Parameters in the Numerical Experiment

Variable	Distribution	Statistics				Source of data
		Mean	Standard deviation	Minimum	Maximum	
RT (m)	Normal	24.5	4.5	5.7	42.6	Carrier et al. (2011)[a]
RST (m)	Uniform	—	—	0.5	5	Chilton and Foster (1995), Fookes (1997)
LSf (—)	Uniform	—	—	0.3	0.5	Chilton and Foster (1995)[b]
SRf (—)	Uniform	—	—	0.8	1.2	Chilton and Foster (1995)[c]
wtD (m)	Uniform	—	—	1.5	20	Carrier et al. (2011)[d]
K_{min} (m/s)	Uniform	—	0.3[e]	5.0×10^{-8}	5.0×10^{-7}	Chilton and Foster (1995), McFarlane et al. (1992)
K_{max} (m/s)	Log-normal	1.5×10^{-5}	0.4[e]	2.4×10^{-7}	5.7×10^{-4}	Based on calibration of transmissivity distribution
K_{rock} (m/s)	Log-normal	6.3×10^{-7}	0.2[e]	7.8×10^{-8}	3.9×10^{-6}	Based on calibration of transmissivity distribution
$minn$ (—)	Uniform	—	—	0.001	0.01	Maréchal et al. (2004)[f]
$maxn$ (m)	Uniform	—	—	0.05	0.1	Boisson et al. (2015), Courtois et al. (2010)
bhD (m)	Uniform	—	—	20	90	Carrier et al. (2011)[g]
$rech$ (mm/year)	Uniform	—	—	10	250	Carrier et al. (2011)[h]
$aqLE$ (m)	Uniform	—	—	100	3,000	Collins et al. (2020)

[a]Carrier et al. (2011) report an average value equal to 24.4 m in 220 boreholes screened in regolith and Precambrian basement bedrock. The corresponding 95% range of the distribution is between 2.2 and 44.6 m. [b]The range is based on data from different African countries, which indicate that the maximum thickness of the lower saprolite layer is about 20 m while that of the upper saprolite is 30 m (i.e., $LSf = 0.4$). [c]The range is based on data from different African countries, which indicate that the maximum thickness of the lower saprolite layer and that of the saprock are similar (i.e., $SRf = 1.0$). [d]Carrier et al. (2011) report an average value equal to 8.1 m and a range between 1.7 and 19.4 m based on data from in 220 boreholes screened in regolith and Precambrian basement bedrock. [e]Log-transformed values. [f]Maréchal et al. (2004) report a value of 0.004 for the average specific yield of a fractured crystalline rock aquifer in India. [g]The data set analyzed by Carrier et al. (2011) has average borehole depth of 51 m in northern Ghana (4,860 boreholes) and a 95% probability range between 22.3 and 90 m. [h]Carrier et al. (2011) analyzed the results of recharge estimations from 15 different studies in West Africa. The resulting range of recharge values is 13–205 mm/year. Recharge is applied only for four stress periods (4 months total).

parameters. To quantify this variability, we defined the variable ΔY as the relative change in maximum sustainable yield after 4 years of continuous pumping:

$$\Delta Y = \frac{Y_{5yr} - Y_{1yr}}{Y_{1yr}} \tag{6}$$

where Y_{1yr} is the maximum allowable yield at the end of the warm-up period for the simulation and Y_{5yr} is corresponding value at the end of the simulation. A positive ΔY indicates that early abstraction rates are not only sustainable, but also there is surplus of water from recharge, storage, or baseflow from fractured basement rock. Conversely, a deficit of groundwater is indicated by $\Delta Y < 0$, while ΔY around zero indicates that the abstractions at the beginning of the simulations are sustainable.

3.4. Global Sensitivity Analysis

The generated synthetic data set of maximum allowable yields was considered for global sensitivity analysis (Pianosi et al., 2016; Saltelli et al., 2008) using the PAWN method (Pianosi et al., 2015; Pianosi & Wagener, 2015, 2018). The PAWN method measures sensitivity of a certain input parameter X_i by comparing the cumulative distribution function (CDF) of the model outputs when all the parameters are free to vary (the unconditional CDF), to the CDF when X_i is fixed (the conditional CDF). If the two distributions are similar or identical in a statistical sense, then parameter X_i has little or no effect on the model output. Assuming $F_Y(Y)$ is the unconditional CDF of the modeling output Y, and $F_{Y|X_i}(Y)$ is the conditional CDF, the sensitivity of an input parameters is quantified by the so-called PAWN index S_i (Pianosi & Wagener, 2015):

$$S_i(X_i) = \max_{X_i} [KS(X_i)] \tag{7}$$

$KS(X_i)$ in Equation 6 is the Kolmogorov-Smirnov (KS) statistic, which is defined as

$$KS(X_i) = \max_Y [F_Y(Y) - F_{Y|X_i}(Y)] \tag{8}$$

The PAWN sensitivity index S_i takes values between 0 (zero influence) and 1 (highest sensitivity).

Sensitivity indices for the 13 model parameters in Tables 1 and 2 were calculated following the procedure described by Pianosi and Wagener (2018) using MATLAB/OCTAVE scripts (Pianosi et al., 2015). Bootstrapping was applied to calculate confidence intervals around the calculated sensitivity indices, while a dummy parameter (i.e., an influential parameter) was added to the analysis to estimate the robustness of the calculated $S_i^{\cdot}$ (Pianosi & Wagener, 2018; Zadeh et al., 2017).

The PAWN method allows the sensitivity analysis to focus on specific subsets of output values (Pianosi & Wagener, 2016). In order to understand the influence of the model parameters on different classes of aquifer productivity, the synthetic data set of maximum allowable yields was split into subsets according to threshold values used by (MacDonald et al., 2012) to map the productivity of different regions in Africa. This classification includes a "very low productivity" class with yields below 6 L/min; a "low productivity" class with yields between 6 and 30 L/min; a "low-moderate productivity" class with yields between 30 and 60 L/min; a "moderate productivity" class with yields between 60 and 300 L/min; and a "high productivity" class with yields above 300 L/min.

4. Results

4.1. Average Maximum Allowable Yields and Model Validation

The CDF of distribution of the average maximum allowable yields shows that 95% of the data are between 5 and 192 L/min (Figure 4a). The mean and median values are equal to 52 and 36 L/min, indicating that the distribution is skewed toward low yield values. Simulated low productivity boreholes (<30 L/min) account for almost 40% of the synthetic data, while data samples representing high yields (>300 L/min) are scarce (1%). Values representing low-moderate and moderate productivity boreholes account for about 30% each. Descriptive statistics for the simulated data set are presented in Table 3, where they are compared to corresponding values from the validation data collected by Carrier et al. (2011). To make this comparison, the simulated data were truncated with a cutoff at 6 L/min to be consistent with the way the reference data are reported by Carrier et al. (2011). The differences between the mean, the standard deviation, and the percentiles of the two distributions are within a few L/min, while the median of the synthetic data is only slightly greater (by 7 L/min). The statistical similarity between simulated and actual yield data is confirmed by the striking match between the empirical CDFs of the synthetic and reference data (Figure 4a) and by the outcome of a two-sample KS test (see Equation 7). Another comparison between the histogram of the simulated yield data, binned into the five classes of productivity, and the histogram of yield data (Bonsor & MacDonald, 2010) from more than 2,000 boreholes in 12 African countries, including Ghana and some in eastern and southern Africa, is shown in Figure 4b. There is an overall good match in the frequencies of the different classes in the two sets of data, although there are some discrepancies in the tails of the distributions (Figure 4b). In particular, the Bonsor and MacDonald (2010) borehole data have a higher percentage of high productive and a lower percentage of low productive boreholes. However, these discrepancies are minor (around 4%) and may reflect the greater occurrence of highly productive fractures in WBAs in some regions (Maurice et al., 2019).

4.2. Transmissivity of the Simulated WBA Profiles

The histogram of estimated equivalent transmissivities (T_{eq}) for the generated WBA profiles is shown in Figure 4c. The calculated T_{eq} values present a log-normal distribution with 95% of the values falling between 4 and 49 m^2/day, a geometric mean equal to 13 m^2/day, and an arithmetic mean equal to 16 m^2/day. For comparison, Carrier et al. (2011) reported a value of 17 m^2/day for the (arithmetic) mean of the transmissivities estimated from 16 pumping tests in the Precambrian basement aquifer in northern Ghana. Several other studies also report transmissivity within the range of T_{eq} values for the simulated profiles (Chilton & Foster, 1995; Holland, 2012; Howard et al., 1992; Taylor & Howard, 2000; Taylor et al., 2010).

In order to understand the relationship between the classes of productivity and T_{eq}, the empirical CDFs of transmissivity values were calculated for different classes of simulated maximum allowable yield values (Figure 4d). The minimum, mean, median, and 95% range (i.e., 2.5th and 97.5th percentiles) values for each subsample are presented in Table 4. Calculated mean transmissivity values for each class of productivity increase from about 6 m^2/day for very low productivity boreholes up to about 74 m^2/day for high productivity.
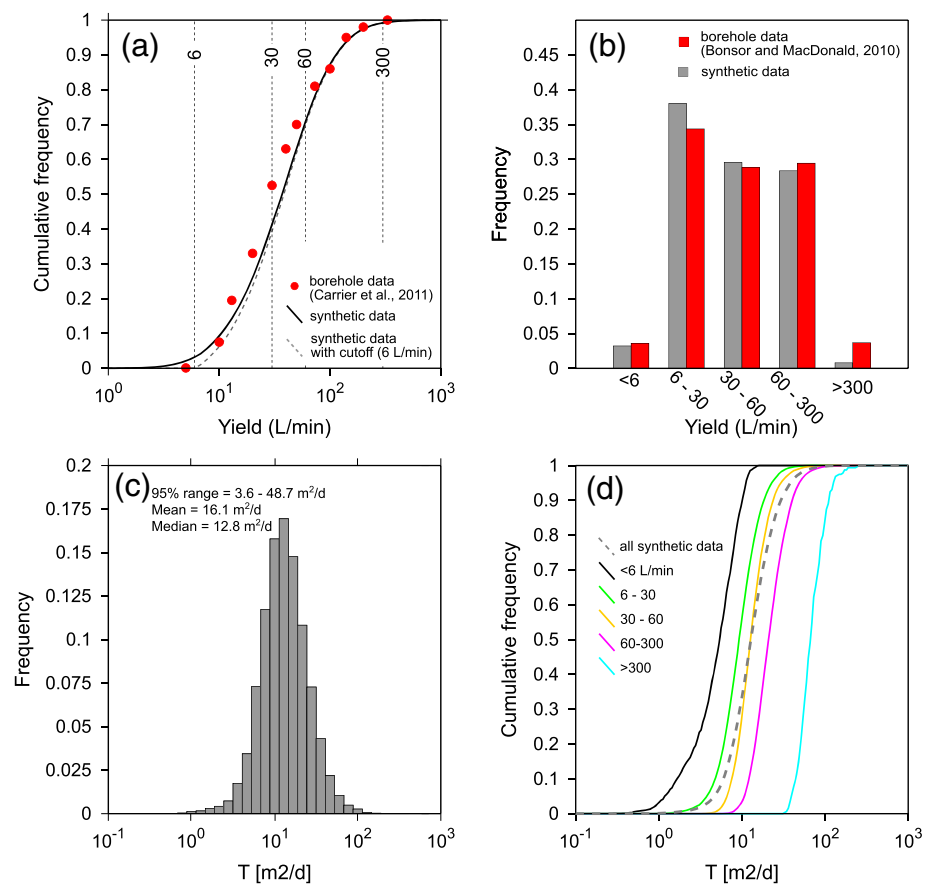
Figure 4. (a) Empirical cumulative distributions for the simulated yields and the validation data. (b) Histogram of simulated yield data binned into five classes of productivity and comparison with the data from Bonsor and MacDonald (2010). (c) Histogram of the computed equivalent transmissivity for the generated profiles. (d) Empirical cumulative distributions of the equivalent transmissivity for different productivity classes.

Table 3
Comparison Between Simulated and Reference Yield Data

Statistics	Carrier et al. (2011) data[a]	Synthetic data
Mean yield (L/min)	52	53
Standard deviation (L/min)	56	55
Median (L/min)	30	37
p2.5% (L/min)	10	8
p97.5% (L/min)	200	195
Probability yield <13 L/min	0.11	0.12
Probability yield between 13 and 70 L/min	0.68	0.66
Probability yield between 70 and 180 L/min	0.16	0.19
Probability yield >180 L/min	0.04	0.03

	Percentage of boreholes	
Borehole productivity	Bonsor and MacDonald (2010) data[b]	Synthetic data
Very low productivity (<6 L/min)	4	3
Low productivity (6–30 L/min)	34	38
Low-moderate productivity (30–60 L/min)	29	30
Moderate productivity (60–300 L/min)	29	28
High productivity (>300 L/min)	4	1

[a]Based on 2,274 boreholes in 12 African countries. [b]Based on 576 boreholes in the Precambrian basement aquifer in northern Ghana.

Table 4
Statistics of Estimated Equivalent Transmissivity (T_{eq}) for Different Classes of Borehole Productivity

Borehole productivity	Minimum	Mean	Median	95% range
Very low productivity (<6 L/min)	0.2	5.7	5.4	0.9–12.0
Low productivity (6–30 L/min)	0.7	10.4	9.0	2.7–24.0
Low-moderate productivity (30–60 L/min)	3.1	14.7	12.7	5.9–36.7
Moderate productivity (60–300 L/min)	4.8	24.4	20.9	9.5–58.9
High productivity (>300 L/min)	32.4	73.5	66.8	36.8–152.2

Note. Values in m^2/day.

4.3. Sensitivity of Simulated Average Maximum Allowable Yields

The global sensitivity of the computed mean maximum allowable yields with respect to the 13 model input parameters is presented in Figure 5. Computed PAWN sensitivity indices, considering the entire synthetic data set, indicate that the most influential parameters for aquifer productivity are the K around the interface between the regolith and the SR (K_{max}), and RT. The depth of the water table (wtD), the equivalent K of the FR (K_{rock}), and the depth of the borehole (bhD) are also relatively highly influential parameters. Other parameters including the thickness of RS (RST), the lateral extent of the regolith and SR layers ($aqLE$), and the ratio between the thicknesses of SR and LS layers (SRf) are less influential. The remaining input parameters are assumed as potentially uninfluential as their PAWN index is similar to that of the dummy parameter, which means that it not possible to distinguish their sensitivity from approximation error (Pianosi & Wagener, 2018).

PAWN sensitivity indices were also computed for subsamples resulting from grouping of the average maximum allowable yield data into classes of productivity (Figure 5). Although there is a consistency between the different classes regarding which parameters are the most influential, the ranking of these parameters varies for the different subsamples. For instance, wtD is a highly influential factor only for the very low (<6 L/min) or high yields (>300 L/min). For all the classes of productivity, RT and K_{max} are consistently the most influential parameters on the variability of the simulated maximum allowable yields.

While PAWN indices quantify the influence of the different parameters on the variability of the model outputs, scatterplots allow insight into the direct or inverse relationships between a certain parameter and the model output. This type of plot is shown in Figure 6, where different parameter samples are plotted against K_{max} values and different classes of productivity are coded using different colors. The clustering of dots with the same colors in Figure 6a confirms the results of the sensitivity analysis and indicates that higher productivity is associated with higher K_{max} values and, to a lesser degree, higher K_{rock} values. The interplay between RT, K_{max}, and the borehole productivity shown in Figure 6b confirms previous indications that the thickness of the regolith is a major factor for the success rate of boreholes in WBAs (e.g., Chilton & Foster, 1995) and
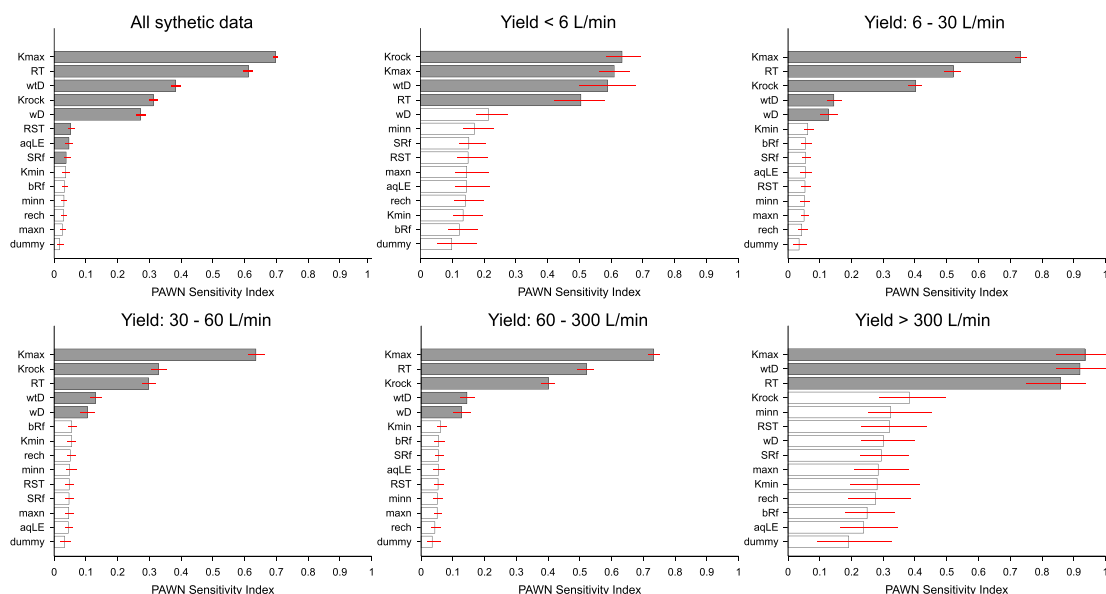

Figure 5. PAWN sensitivity indices for the average maximum allowable yields. The red lines represent the 95% confidence intervals calculated by bootstrapping. White bars indicate noninfluential parameters.
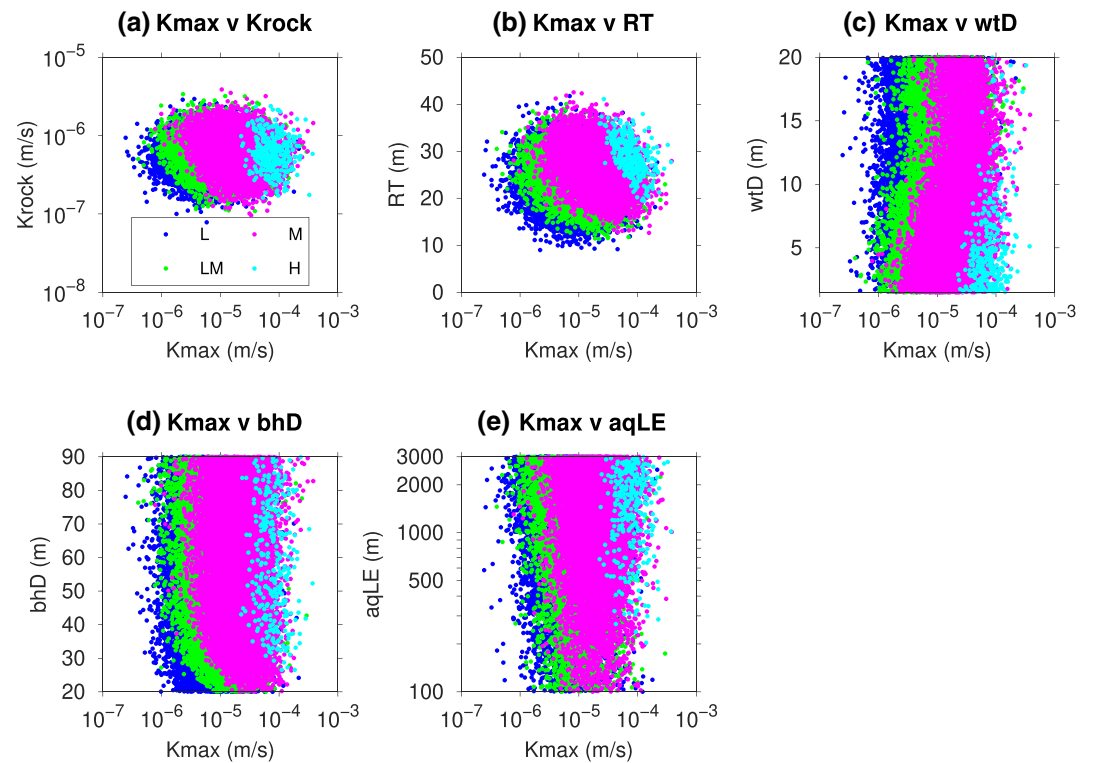
Figure 6. Scatterplots comparing K_{max} to other input parameters. Colors correspond to average maximum yield values classified into four classes of productivity (L = low yield, 6–30 L/min; LM = low-moderate yield, 30–60 L/min; M = moderate yield, 60–300 L/min; H = high yield >300 L/min).

that low productivity values are generally the result of a thinner less conductive regolith. As shown by the ranking of the PAWN indices, the water table depth also influences productivity especially for the low and high classes (Figure 6c). In particular, when the water table is deep (>15 m below surface), results show that there is a very low chance of high productivity even for highly permeable WBA profiles. Conversely, if the water table is shallow (<5 m) there is high probability of low-moderate and moderate productivity values. Figure 6d indicates that *bhD* is a factor only for the productivity of shallow boreholes (<30 m) and has no influence for deeper boreholes. Regardless of the K of the WBA profile, results also show that there is higher chance of moderate to high productivity from aquifers that have a greater lateral extent (Figure 6e).

4.4. Sensitivity of Variations in Maximum Allowable Yields After 4 Years of Pumping

The results of the global sensitivity analysis of the considered parameters with respect to changes in yield ΔY (Figure 7) indicate that the most influential parameters for the sustainability of the simulated abstractions after 1 year of pumping are, in the following order, *aqLE*, K_{rock}, *wtD*, and *bhD*. Other particularly influential parameters are the net recharge rate (*rech*) and *RT*. Porosity parameters (*maxn* and *minn*), which were not influential with respect to the maximum allowable yield, become influential for determining the sustainability of the abstractions although in a relatively minor role. From the PAWN index of the dummy variable, the only noninfluential parameters are *SRf* and the K_{min}. As for the average productivity, the ranking of the parameters changes when we consider different classes of aquifer productivity. For instance, for boreholes providing yields in the 6–30 L/min range, the most influential parameters are those controlling the K of the profile (K_{max} and K_{rock}) and *rech*. As yields grow, so does the influence of factors like *wtD* and *aqLE*.

Further considerations regarding the sustainability of the calculated yields can be drawn from the scatterplots in Figure 8. The comparison between simulated maximum allowable yields after 1 year of simulation (Y_{1yr}) and after 5 years (Y_{5yr}) shows that the majority of the early moderate to high yields cannot be continuously sustained over the considered period (Figure 8a), since the simulated abstraction rates decreased over time to maintain the groundwater level in the borehole equal to the imposed h_{min} level. Sustainability,
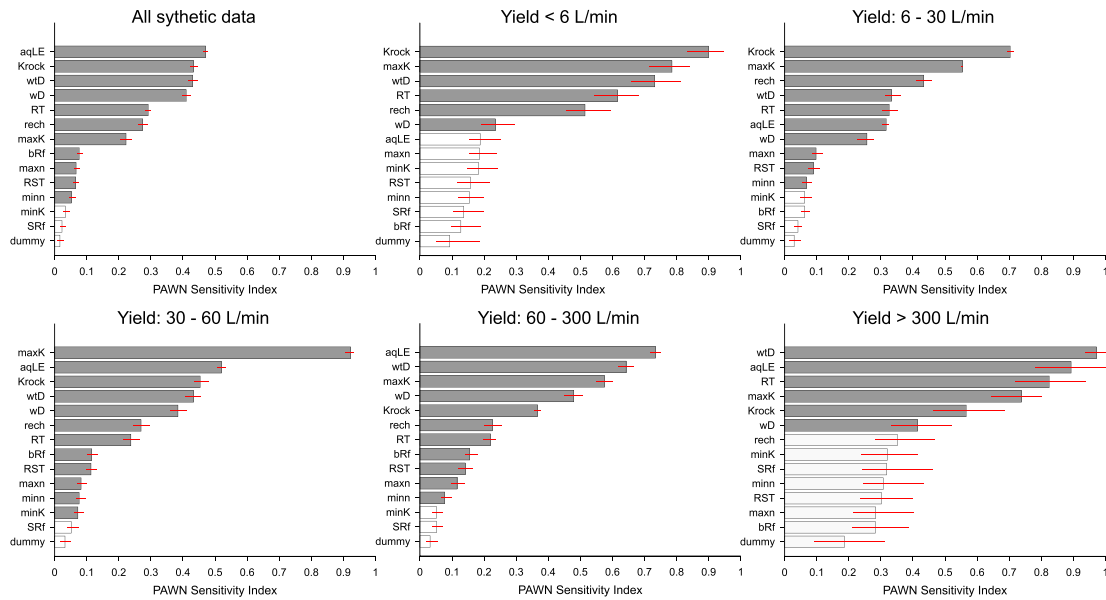
Figure 7. PAWN sensitivity indices for the variable ΔY. The red lines represent the 95% confidence intervals calculated by bootstrapping. White bars indicate noninfluential parameters.
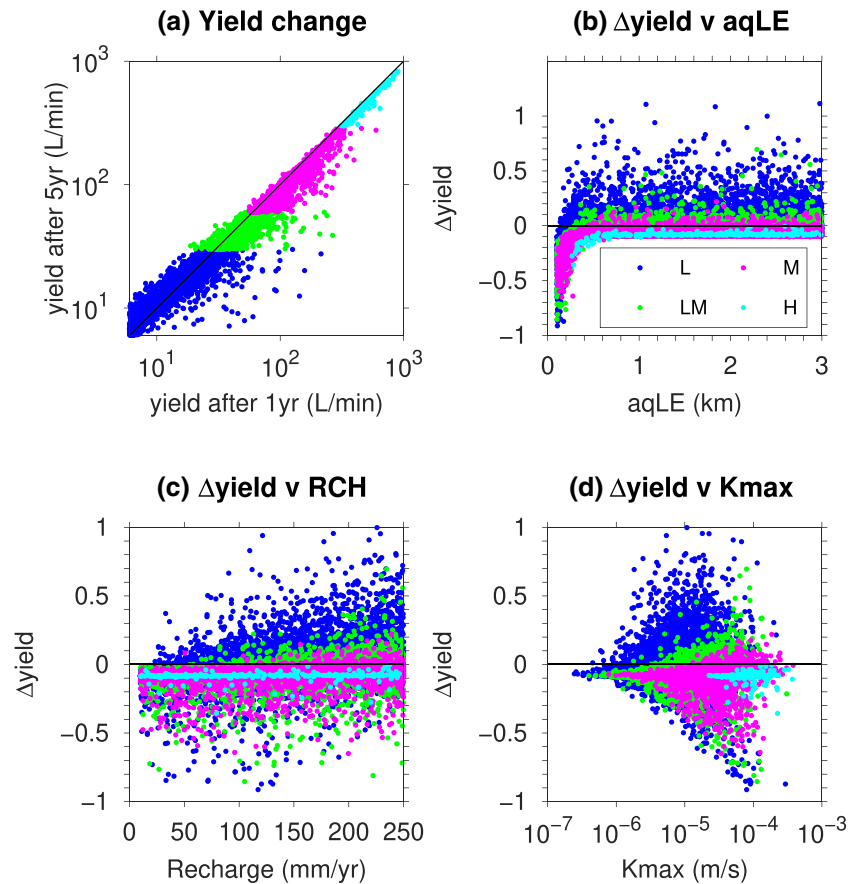

Figure 8. Sustainability of the simulated maximum yields. Colors correspond to average maximum yield values classified into four classes of productivity (L = low yield, 6–30 L/min; LM = low-moderate yield, 30–60 L/min; M = moderate yield, 60–300 L/min; H = high yield >300 L/min). (a) Comparison between simulated yields at the beginning and at the end of the simulation. (b–d) Scatterplots where the change in yield is plotted against a certain input parameter.

which is indicated by positive ΔY values, tends to increase with $aqLE$ (Figure 8b). For low and low-moderate productivity boreholes, ΔY values are mostly positive showing a surplus of water after 4 years; initial yields become unsustainable only for $aqLE$ less than 150–200 and 400 m, respectively. Almost none of the initial high productive yields measured after 1 year are sustained in the long term ($\Delta Y < 0$) but experience a drop in yield of 9% on average after 4 years. As expected, $rech$ exerts a positive impact on sustainability (Figure 8c). For low productivity boreholes (6–30 L/min), initial yields can be sustained for $rech$ values as low as 15–20 mm/year. In the case of intermittent pumping, which is typical for hand pumps, a lower threshold is expected depending on the duration of the production period. Detailed analysis of the influence of intermittent pumping will be the topic of a follow-up study. The combination of net recharge and aquifer length can determine the long-term sustainability of the abstractions. For low-moderate productivity boreholes and aquifer lengths in the order of 500 m, the critical $rech$ value for sustain the initial yields is around 75 mm/year. The critical $rech$ value reduces for larger $aqLE$, and it is around 50 mm/year for $aqLE$ in the order of 3 km. For all the productivity classes, sustainability increases with the hydraulic conductivity of the profiles as shown in Figure 8d.

5. Discussion

5.1. Representativity of the Simulated WBA Profiles and Maximum Allowable Yields

The main objective of the numerical experiment was to generate a large set of borehole yield data that could be used to understand which parameters have greater control on groundwater productivity. The close match between simulated and reference data from northern Ghana (Tables 3 and 4 and Figure 4) demonstrates that by parameterizing the developed stochastic numerical model with realistic ranges of geological, hydrogeological, recharge, and borehole construction data, it was possible to retrieve a distribution of simulated yields that is statistically very similar to actual borehole data. This result gives confidence in the insights from the interpretation of the sensitivity analysis of the generated data set and the influence of different parameters on borehole productivity. Further, the match between the synthetic yield data derived for northern Ghana and collated measured yield data for WBA settings across sub-Saharan Africa confirms the suitability of the model for wider geographical application.

Nonetheless, the presented modeling approach has some limitations that have to be considered in the assessment of the results and wider applicability. One potential limitation is the chosen conceptual model for generating realizations of aquifer heterogeneity (Figure 2). Although the conceptual profile proposed by Chilton and Foster (1995) provides a generally accepted description of the broad structure of a generic WBA, it presents smooth variations of hydraulic conductivity and porosity with depth, which may underestimate the actual degree of heterogeneity. Hydraulic testing in WBAs and in other types of aquifers has shown that the vertical changes in conductivity can be abrupt (Bohling et al., 2016; Bonsor et al., 2014), as in the case of very conductive individual fractures, which may require more complex conceptualizations of the aquifer heterogeneity (Dewandel et al., 2006). However, the stochastic modeling approach developed here is sufficiently flexible that can be applied to templates and conceptualisations describing different or more complex settings. A limitation of the current modeling approach that will be explored in future developments is the impact of horizontal variability in the hydrogeological parameters on aquifer productivity, for instance, where the degree of weathering varies spatially due to geologic or tectonomorfic factors.

Regarding the reliability of the modeling outputs, the estimated maximum allowable yields have to be considered optimal values in the best-case scenario in which the hydraulic efficiency of the borehole is 100%. The borehole is also assumed to be operated in an optimal way, such that the abstraction rate is constantly adjusted according to the water level in the borehole and the depth of the most productive horizon (Equation 4). Calculated threshold values for the minimum transmissivity of the profile, the minimum net recharge, and the minimum aquifer extension for the different classes of productivity refer to the case of continuous groundwater abstraction, while lower thresholds need to be considered for intermittent pumping. The way aquifer recharge is simulated in the model is another potential limitation, which may affect considerations regarding the sustainability of the estimated yields. The climatic signal was simply simulated as a constant net recharge influx active over the 4 months of a wet season. The climatic signal was simply simulated as a constant net recharge influx active over the 4 months of a wet season. In reality, the response of recharge to rainfall is likely more complex and nonlinear (Acworth, 2019), as in areas where recharge is

associated with intense rainfall such as in dry subtropical locations (Cuthbert et al., 2019) where more complex representation of the climatic control on the simulated abstractions may be needed (e.g., Ascott et al., 2019).

5.2. Controlling Factors on WBA Productivity and Sustainability of the Abstractions

As expected, estimated higher maximum allowable yields are associated with higher transmissivity values (Table 4 and Figure 4d). For the subsample of T_{eq} values corresponding to low productivity boreholes, a value of 2.7 m^2/day was found as the threshold below which boreholes cannot sustain a continuous abstraction with an average constant rate greater than 6 L/min (8.6 m^3/day). However, in many communities, daily pumping is much less than this, given that pumps rarely operate for more than 12 hr and pumping is not continuous (MacDonald et al., 2008; Thomson et al., 2019). Therefore, for a daily pumped volume of 4.3 m^3, transmissivity values of approximately 1.4 m^2/day may be sufficient.

In sub-Saharan Africa and other parts of the developing world there is growing interest in the adoption of solar photovoltaic cells for powering groundwater pumps (Agrawal & Jain, 2019; Chandel et al., 2015; Wazed et al., 2018). The main target for these systems is smallholder irrigation, which requires discharge rates in the order of 30 L/min and above (MacDonald et al., 2012). The comparison between estimated transmissivity values and corresponding simulated allowable yields suggests that the threshold transmissivity for delivering such rates is in the order of 6 m^2/day, while higher water demand (>300 L/min) requires transmissivities of at least 37 m^2/day.

Computed PAWN sensitivity indices, considering the entire synthetic data set, indicate that the most influential parameters for aquifer productivity are the hydraulic conductivity around the interface between the regolith and the saprock (K_{max}) and the thickness of the regolith (RT). This result highlights the importance of site-specific hydrogeological characterization studies as well as assessments of the nature and the maturity of the weathering profile for borehole siting and productivity considerations. The use of geophysical methods to help target areas of thickest weathering and fracture zones is well established (Acworth, 2019; Hazell et al., 1988), and this study demonstrates the value of such approaches when well applied.

The analysis of the relationships between the values of the most influential parameters and the classes of productivity (Figure 6) helps to identify important threshold values. For instance, the comparison between productivity and reference conductivity values of the regolith/saprock interface (K_{max}) and of the unweathered crystalline basement (K_{rock}) suggests that boreholes in WBAs can only supply moderate productivity yields (60–300 L/min) for K_{max} values as low as 10^{-6} m/s if there is sufficient flow within the unweathered basement, which has to have comparable conductivity; this is possible in some geological environments such as some metamorphic terrains (Collins et al., 2020). If the equivalent K of the unweathered basement is 1 order of magnitude lower ($\approx 10^{-7}$ m/s), then K_{max} of the aquifer has to increase approximately by at least 1 order of magnitude (>10^{-5} m/s) to sustain moderate yields. For K_{max} values below 10^{-6} m/s, productivity is low regardless of K_{rock}. Similarly, when K_{max} is in the order of 10^{-4} m/s, the WBA can sustain higher abstractions above 300 L/min. For the range of K_{max} values considered in our numerical analysis, productivity above 60 L/min cannot be sustained if the thickness of the regolith layer is less than about 15 m; this threshold rises to about 20 m for high productivity boreholes. By combining the observations for RT and wtD, we can conclude that a thick (>15 m), saturated (<5 m) regolith provides ideal conditions for groundwater development in WBAs.

Another factor that can affect the productivity of boreholes in WBA is the lateral extension of the aquifer. This parameter can be interpreted as the location of a physical lateral boundary for the regolith or a groundwater divide. In the latter case, the model output provides an indication of the minimum distances between boreholes, although superposition effects should be considered for more accurate estimations. For African weathered terrains, lateral continuity is generally a function of the age of the weathering surface, which in turn controls the duration of the exposure (Burke & Gunnell, 2008). Thicker and more laterally persistent WBAs are to be expected across the older surfaces, while WBAs produced by relatively recent and more active surfaces, as in northern Ghana, tend to be more discontinuous (Jones, 1985). For the simulated case study, results suggest that when the conductivity of the productive layer is sufficiently high ($K_{max} > 10^{-6}$ m/s), low abstraction rates such as those from hand pumps can be sustained for aquifer extensions as low as approximately 200 m (borehole separation of 400 m) and total net recharge rates of about 30 mm/year

(Figure 8). Low to moderate abstractions can be sustained for aquifer extensions as low as 300 m if the net recharge in the aquifer is above 50 mm/year. Higher productivity from the simulated WBAs is sustainable only for highly conductive profiles ($K_{max} > 10^{-5}$ m/s), recharge rates in the order of 100 mm/year or above, and aquifer extensions greater than 400 m. In general, greater aquifer extensions require lower recharge rates.

5.3. Implications for African Water Supply From WBAs

The numerical experiment highlights that for the conditions in the weathered basement of northern Ghana, well-sited boreholes can easily sustain yields of 6 L/min equivalent to a hand pump. The thickness of the regolith and the maximum hydraulic conductivity developed at the base of the saprolite are the critical factors controlling success. Fitting these boreholes with higher yielding pumps significantly reduces the success rate. Only 28% of boreholes could sustain a yield of above 60 L/min and 1% a yield greater than 300 L/min. Also, at higher yields, the aquifer extent and recharge become much more significant for longer-term sustainability. This has obvious implications for the viability of initiatives to extend reticulated water supply schemes in crystalline basement aquifers or increased use of groundwater for irrigation. Higher yielding boreholes are possible but rare and will require much greater investment in both siting/exploration and in the construction, requiring deeper boreholes (>70 m) or the penetration into the unweathered crystalline rock to access productive fractures, with a greater risk of failure. Current initiatives to use solar energy should also recognize the physical limitations of higher yielding pumps despite the availability of energy and promote the use of much lower yielding pumps.

6. Summary and Conclusions

WBAs are a strategic water resource in most sub-Saharan African countries and in arid and semiarid regions around the world, and there is growing demand to increase abstraction to meet water and food security needs (Cobbing, 2020). In this work, we have demonstrated that the productivity and sustainability of groundwater abstractions can be reliably investigated with a numerical approach to generate representative profiles of aquifer heterogeneity and an axisymmetric transient groundwater flow model. This approach was applied in a numerical experiment in which a sample of 13 model input parameters was generated to represent the range of values observed in borehole data and field tests in the Precambrian WBA in northern Ghana. The distribution of the resulting data set of simulated maximum allowable yields was compared to the distribution of measured yield data, showing a very good agreement. This result indicates that when representative sets of input parameters for a certain WBA are fed into the developed stochastic model, it is possible to retrieve reliable estimates of borehole productivity.

The validated synthetic data set was further analyzed in order to understand the influence of different input parameters on borehole productivity and sustainability of the abstractions. The results of a global sensitivity analysis indicated that the most influential parameters for borehole productivity are those controlling the hydraulic conductivity profile of the regolith and saprock, the thickness of the weathered profile, and the depth of the water table. These results confirm the importance of local hydrogeological characterization and assessments of the nature of the weathered profile for borehole siting.

The synthetic data set also allowed the relationships between parameters and productivity to be examined. As expected, there is a direct relationship between the equivalent transmissivity of the WBA and borehole productivity. The analysis of simulated data indicates that WBA profiles with transmissivities as low as 2.7 m^2/day can provide enough groundwater to sustain a continuous abstraction with an average constant rate of at least 6 L/min. For hand pumps and intermittent pumping, the transmissivity threshold is expected to be even lower, in order of 1.4 m^2/day. Results also suggest that transmissivities as low as about 6 m^2/day might allow the full abstraction potential of solar-powered pumps (yield >30 L/min) to be met. There is growing investment being undertaken in this technology in Africa for irrigation purposes, but a recognition that limited attention has been applied to the sustainable borehole yields that can be achieved (Agrawal & Jain, 2019; Aliyu et al., 2018; Closas & Rap, 2017; Schmitter et al., 2018). Moderate and high yields may require transmissivity values higher than 9 and 37 m^2/day, respectively.

With respect to the hydraulic conductivity of the productive zone at the boundary between the LS and saprock layers, a value in the order of 10^{-6} m/s was estimated as the threshold for low and low-moderate

productivity (<30 L/min). Abstractions above 300 L/min can only be sustained when the conductivity of the productive zone is in the order of 10^{-4} m/s. Comparisons between regolith thickness, water table depth, and simulated yields indicate a direct relationship between productivity and these parameters. As a general rule, the analysis of the simulated data shows that a thick (>15 m) and saturated (>5 m) regolith are ideal conditions for groundwater development in WBAs.

The analysis of temporal changes in the simulated yields for the analyzed case study reveals that initial moderate to high abstraction rates are generally not sustainable in the long period but can reduce by 9% on average after 4 years. Sustainability of initial rates over the simulated period is affected by several parameters, some of which were not highly influential in the sensitivity analysis of borehole productivity. These parameters include borehole depth, net recharge, and lateral extension of the aquifer. Critical values of aquifer extension of approximately 200, 300, and 400 m seem to define the thresholds for sustainable low, low-moderate, and moderate abstractions, respectively.

The validated synthetic data set demonstrates that in the WBA of northern Ghana, well-sited boreholes can very likely sustain the yield of a hand pump (6 L/min). However, only about 30% of these boreholes could support moderate yields in excess of 60 L/min, and only about 1% yield higher than 300 L/min. Moderate yields would require at least an aquifer extent of about 400 m and an average annual net recharge of 100 mm/year to be sustainable over 4 years. These conditions may pose serious challenges to the widespread conversion of higher yielding pumps (through solar energy or conventional) in sub-Saharan Africa.

Although the proposed modeling approach was able to reproduce the reference borehole data from northern Ghana with good accuracy, further testing is needed in other countries where WBAs provide a significant water resource. In particular, different conceptualizations of the heterogeneity profile could be developed and integrated in the stochastic modeling framework. This work mainly focused on the impact of structural and hydrogeological parameters on groundwater productivity and sustainability. The effects of borehole design and operation (e.g., well losses and intermittent pumping) and changes in the climatic signal (e.g., different recharge patterns) will be integrated in future developments.

Data Availability Statement

The synthetic data set of simulated yields and transmissivities can be downloaded from the National Geoscience Data Centre of the British Geological Survey (https://www.bgs.ac.uk/services/ngdc/accessions/index.html#item136651; the data set DOI is 10.5285/67c00a03-9de2-4e3a-97ad-ac330b668904).

References

Acheampong, S. Y., & Hess, J. W. (1998). Hydrogeologic and hydrochemical framework of the shallow groundwater system in the southern Voltaian Sedimentary Basin, Ghana. *Hydrogeology Journal*, *6*(4), 527–537. https://doi.org/10.1007/s100400050173

Acworth, I. (2019). *Investigating groundwater*. London: CRC Press. https://doi.org/10.1201/9781351008525

Acworth, R. I. (1981, July). The evaluation of groundwater resources in the crystalline basement of northern Nigeria (PhD Thesis). University of Birmingham. Retrieved from https://etheses.bham.ac.uk/id/eprint/3576/

Acworth, R. I. (1987). The development of crystalline basement aquifers in a tropical environment. *Quarterly Journal of Engineering Geology and Hydrogeology*, *20*(4), 265–272. https://doi.org/10.1144/GSL.QJEG.1987.020.04.02

Agrawal, S., & Jain, A. (2019). Sustainable deployment of solar irrigation pumps: Key determinants and strategies. *Wiley Interdisciplinary Reviews: Energy and Environment*, *8*, e325. https://doi.org/10.1002/wene.325

Ahmed II, J. B., & Mansor, S. (2018). Overview of the application of geospatial technology to groundwater potential mapping in Nigeria. *Arabian Journal of Geosciences*, *11*, 504. https://doi.org/10.1007/s12517-018-3852-4

Aliyu, M., Hassan, G., Said, S. A., Siddiqui, M. U., Alawami, A. T., & Elamin, I. M. (2018). A review of solar-powered water pumping systems. *Renewable and Sustainable Energy Reviews*, *87*, 61–76. https://doi.org/10.1016/j.rser.2018.02.010

Altchenko, Y., & Villholth, K. G. (2015). Mapping irrigation potential from renewable groundwater in Africa—A quantitative hydrological approach. *Hydrology and Earth System Sciences*, *19*, 1055–1067. https://doi.org/10.5194/hess-19-1055-2015

Ascott, M. J., Mansour, M. M., Bloomfield, J. P., & Upton, K. A. (2019). Analysis of the impact of hydraulic properties and climate change on estimations of borehole yields. *Journal of Hydrology*, *577*, 123998. https://doi.org/10.1016/j.jhydrol.2019.123998

Ayraud, V., Aquilina, L., Labasque, T., Pauwels, H., Molenat, J., Pierson-Wickmann, A.-C., et al. (2008). Compartmentalization of physical and chemical properties in hard-rock aquifers deduced from chemical and groundwater age analyses. *Applied Geochemistry*, *23*(9), 2686–2707. https://doi.org/10.1016/j.apgeochem.2008.06.001

Barker, R. D., White, C. C., & Houston, J. F. T. (1992). Borehole siting in an African accelerated drought relief project. *Geological Society, London, Special Publications*, *66*(1), 183–201. https://doi.org/10.1144/GSL.SP.1992.066.01.09

Belle, P., Lachassagne, P., Mathieu, F., Barbet, C., Brisset, N., & Gourry, J.-C. (2019). Characterization and location of the laminated layer within hard rock weathering profiles from electrical resistivity tomography: Implications for water well siting. *Geological Society, London, Special Publications*, *479*, 187–205. https://doi.org/10.1144/SP479.7

Bohling, G. C., Liu, G., Dietrich, P., & Butler, J. J. (2016). Reassessing the MADE direct-push hydraulic conductivity data using a revised calibration procedure. *Water Resources Research*, *52*, 8970–8985. https://doi.org/10.1002/2016WR019008

Boisson, A., Guihéneuf, N., Perrin, J., Bour, O., Dewandel, B., Dausse, A., et al. (2015). Determining the vertical evolution of hydrodynamic parameters in weathered and fractured south Indian crystalline-rock aquifers: Insights from a study on an instrumented site. *Hydrogeology Journal*, *23*, 757–773. https://doi.org/10.1007/s10040-014-1226-x

Bonsor, H. C., & MacDonald, A. M. (2010). *Groundwater and climate change in Africa: Review of aquifer properties data* (p. 24). Nottingham, UK: British Geological Survey. (IR/10/076) http://nora.nerc.ac.uk/id/eprint/501777/

Bonsor, H. C., MacDonald, A. M., & Davies, J. (2014). Evidence for extreme variations in the permeability of laterite from a detailed analysis of well behaviour in Nigeria. *Hydrological Processes*, *28*, 3563–3573. https://doi.org/10.1002/hyp.9871

Braune, E., & Xu, Y. (2010). The role of ground water in sub-Saharan Africa. *Groundwater*, *48*(2), 229–238. https://doi.org/10.1111/j.1745-6584.2009.00557.x

Burke, K., & Gunnell, Y. (2008). The African erosion surface: A continental-scale synthesis of geomorphology, tectonics, and environmental change over the past 180 million years. In *Memoir 201: The African erosion surface: A continental-scale synthesis of geomorphology, tectonics, and environmental change over the past 180 million years* (Vol. 201, pp. 1–66). Boulder, Colorado: Geological Society of America. https://doi.org/10.1130/2008.1201

Calow, R. C., MacDonald, A. M., Nicol, A. L., & Robins, N. S. (2010). Ground water security and drought in Africa: Linking availability, access, and demand. *Groundwater*, *48*(2), 246–256. https://doi.org/10.1111/j.1745-6584.2009.00558.x

Carrier, M.-A., Aubut, R., Lefebvre, R., Racicot, J., Asare, E. B., Gravel, E., & Rivera, A. (2011). *Hydrogeological assessment project of the northern regions of Ghana (HAP) (Canadian International Development Agency (CIDA) by SNC-Lavalin/INRS joint venture no. R1325)* (p. 236). Québec: Canadian International Development Agency. Retrieved from. http://espace.inrs.ca/1647/1/R001326.pdf

Chandel, S. S., Naik, M. N., & Chandel, R. (2015). Review of solar photovoltaic water pumping system technology for irrigation and community drinking water supplies. *Renewable and Sustainable Energy Reviews*, *49*, 1084–1099. https://doi.org/10.1016/j.rser.2015.04.083

Chandra, S., Ahmed, S., Ram, A., & Dewandel, B. (2008). Estimation of hard rock aquifers hydraulic conductivity from geoelectrical measurements: A theoretical development with field application. *Journal of Hydrology*, *357*(3–4), 218–227. https://doi.org/10.1016/j.jhydrol.2008.05.023

Chilton, P. J., & Foster, S. S. D. (1995). Hydrogeological characterisation and water-supply potential of basement aquifers in tropical Africa. *Hydrogeology Journal*, *3*(1), 36–49. https://doi.org/10.1007/s100400050061

Closas, A., & Rap, E. (2017). Solar-based groundwater pumping for irrigation: Sustainability, policies, and limitations. *Energy Policy*, *104*, 33–37. https://doi.org/10.1016/j.enpol.2017.01.035

Cobbing, J. (2020). Groundwater and the discourse of shortage in sub-Saharan Africa. *Hydrogeology Journal*, *28*(4), 1143–1154. https://doi.org/10.1007/s10040-020-02147-5

Collins, S., Loveless, S. E., Muddu, S., Buvaneshwari, S., Palamakumbura, R. N., Krabbendam, M., et al. (2020). Groundwater connectivity of a sheared gneiss aquifer in the Cauvery River basin, India. *Hydrogeology Journal*, *28*, 1371–1388. https://doi.org/10.1007/s10040-020-02140-y

Courtois, N., Lachassagne, P., Wyns, R., Blanchin, R., Bougaïré, F. D., Somé, S., & Tapsoba, A. (2010). Large-scale mapping of hard-rock aquifer properties applied to Burkina Faso. *Groundwater*, *48*(2), 269–283. https://doi.org/10.1111/j.1745-6584.2009.00620.x

Cuthbert, M. O., Taylor, R. G., Favreau, G., Todd, M. C., Shamsudduha, M., Villholth, K. G., et al. (2019). Observed controls on resilience of groundwater to climate variability in sub-Saharan Africa. *Nature*, *572*, 230–234. https://doi.org/10.1038/s41586-019-1441-7

Dapaah-Siakwan, S., & Gyau-Boakye, P. (2000). Hydrogeologic framework and borehole yields in Ghana. *Hydrogeology Journal*, *8*(4), 405–416. https://doi.org/10.1007/PL00010976

Dewandel, B., Caballero, Y., Perrin, J., Boisson, A., Dazin, F., Ferrant, S., et al. (2017). A methodology for regionalizing 3-D effective porosity at watershed scale in crystalline aquifers. *Hydrological Processes*, *31*, 2277–2295. https://doi.org/10.1002/hyp.11187

Dewandel, B., Jeanpert, J., Ladouche, B., Join, J.-L., & Maréchal, J.-C. (2017). Inferring the heterogeneity, transmissivity and hydraulic conductivity of crystalline aquifers from a detailed water-table map. *Journal of Hydrology*, *550*, 118–129. https://doi.org/10.1016/j.jhydrol.2017.03.075

Dewandel, B., Lachassagne, P., Wyns, R., Maréchal, J. C., & Krishnamurthy, N. S. (2006). A generalized 3-D geological and hydrogeological conceptual model of granite aquifers controlled by single or multiphase weathering. *Journal of Hydrology*, *330*(1–2), 260–284. https://doi.org/10.1016/j.jhydrol.2006.03.026

Edet, A., & Okereke, C. (2005). Hydrogeological and hydrochemical character of the regolith aquifer, northern Obudu Plateau, southern Nigeria. *Hydrogeology Journal*, *13*(2), 391–415. https://doi.org/10.1007/s10040-004-0358-9

Fookes, P. G. (1997). *Tropical residual soils: A Geological Society Engineering Group Working Party revised report*. London: Geological Society of London. https://www.geolsoc.org.uk/PHTRS

Forkuor, G., Pavelic, P., Asare, E., & Obuobie, E. (2013). Modelling potential areas of groundwater development for agriculture in northern Ghana using GIS/RS. *Hydrological Sciences Journal*, *58*, 437–451. https://doi.org/10.1080/02626667.2012.754101

Guihéneuf, N., Boisson, A., Bour, O., Dewandel, B., Perrin, J., Dausse, A., et al. (2014). Groundwater flows in weathered crystalline rocks: Impact of piezometric variations and depth-dependent fracture connectivity. *Journal of Hydrology*, *511*, 320–334. https://doi.org/10.1016/j.jhydrol.2014.01.061

Harbaugh, A. W. (2005). MODFLOW-2005, The U.S. Geological Survey modular ground-water model—the Ground-Water Flow Process: U.S. Geological Survey Techniques and Methods 6–A16, variously p. https://doi.org/10.3133/tm6A16

Hazell, J. R. T., Cratchley, C. R., & Jones, C. R. C. (1992). The hydrogeology of crystalline aquifers in northern Nigeria and geophysical techniques used in their exploration. *Geological Society, London, Special Publications*, *66*(1), 155–182. https://doi.org/10.1144/GSL.SP.1992.066.01.08

Hazell, J. R. T., Cratchley, C. R., & Preston, A. M. (1988). The location of aquifers in crystalline rocks and alluvium in Northern Nigeria using combined electromagnetic and resistivity techniques. *Quarterly Journal of Engineering Geology and Hydrogeology*, *21*(2), 159–175. https://doi.org/10.1144/GSL.QJEG.1988.021.02.05

Holland, M. (2012). Evaluation of factors influencing transmissivity in fractured hard-rock aquifers of the Limpopo Province. *Water SA*, *38*(3). https://doi.org/10.4314/wsa.v38i3.3

Houston, J. F. T., & Lewis, R. T. (1988). The Victoria Province drought relief project, II. Borehole yield relationships. *Groundwater*, *26*(4), 418–426. https://doi.org/10.1111/j.1745-6584.1988.tb00407.x

Howard, K. W. F., Hughes, M., Charlesworth, D. L., & Ngobi, G. (1992). Hydrogeologic evaluation of fracture permeability in crystalline basement aquifers of Uganda. *Applied Hydrogeology*, *1*(1), 55–65. https://doi.org/10.1007/s100400050029

Jones, M. J. (1985). The weathered zone aquifers of the basement complex areas of Africa. *Quarterly Journal of Engineering Geology and Hydrogeology*, *18*(1), 35–46. https://doi.org/10.1144/GSL.QJEG.1985.018.01.06

Lachassagne, P., Wyns, R., Bérard, P., Bruel, T., Chéry, L., Coutand, T., et al. (2001). Exploitation of high-yields in hard-rock aquifers: Downscaling methodology combining GIS and multicriteria analysis to delineate field prospecting zones. *Groundwater*, *39*(4), 568–581. https://doi.org/10.1111/j.1745-6584.2001.tb02345.x

Langevin, C. D. (2008). Modeling axisymmetric flow and transport. *Groundwater*, *46*(4), 579–590. https://doi.org/10.1111/j.1745-6584.2008.00445.x

Long, J. C. S., Remer, J. S., Wilson, C. R., & Witherspoon, P. A. (1982). Porous media equivalents for networks of discontinuous fractures. *Water Resources Research*, *18*(3), 645–658. https://doi.org/10.1029/WR018i003p00645

Louwyck, A., Vandenbohede, A., Bakker, M., & Lebbe, L. (2014). MODFLOW procedure to simulate axisymmetric flow in radially heterogeneous and layered aquifer systems. *Hydrogeology Journal*, *22*, 1217–1226. https://doi.org/10.1007/s10040-014-1150-0

MacDonald, A. M., Barker, J. A., & Davies, J. (2008). The bailer test: A simple effective pumping test for assessing borehole success. *Hydrogeology Journal*, *16*(6), 1065–1075. https://doi.org/10.1007/s10040-008-0286-1

MacDonald, A. M., Bonsor, H. C., Dochartaigh, B. É. Ó., & Taylor, R. G. (2012). Quantitative maps of groundwater resources in Africa. *Environmental Research Letters*, *7*(2), 024009. https://doi.org/10.1088/1748-9326/7/2/024009

MacDonald, A. M., & Calow, R. C. (2009). Developing groundwater for secure rural water supplies in Africa. *Desalination*, *248*(1–3), 546–556. https://doi.org/10.1016/j.desal.2008.05.100

Macdonald, D. M. J., & Edmunds, W. M. (2014). Estimation of groundwater recharge in weathered basement aquifers, southern Zimbabwe; a geochemical approach. *Applied Geochemistry*, *42*, 86–100. https://doi.org/10.1016/j.apgeochem.2014.01.003

Maréchal, J. C., Dewandel, B., & Subrahmanyam, K. (2004). Use of hydraulic tests at different scales to characterize fracture network properties in the weathered-fractured layer of a hard rock aquifer. *Water Resources Research*, *40*, W11508. https://doi.org/10.1029/2004WR003137

Mariethoz, G., & Caers, J. (2014). *Multiple-point geostatistics: Stochastic modeling with training images*. Chichester, UK: John Wiley & Sons, Ltd. https://doi.org/10.1002/9781118662953

Maurice, L., Taylor, R. G., Tindimugaya, C., MacDonald, A. M., Johnson, P., Kaponda, A., et al. (2019). Characteristics of high-intensity groundwater abstractions from weathered crystalline bedrock aquifers in East Africa. *Hydrogeology Journal*, *27*, 459–474. https://doi.org/10.1007/s10040-018-1836-9

McFarlane, M. J., Chilton, P. J., & Lewis, M. A. (1992). Geomorphological controls on borehole yields: A statistical study in an area of basement rocks in central Malawi. *Geological Society, London, Special Publications*, *66*(1), 131–154. https://doi.org/10.1144/GSL.SP.1992.066.01.07

Meju, M. A., Fontes, S. L., Ulugergerli, E. U., Terra, E. F. L., Germano, C. R., & Carvalho, R. M. (2001). A joint TEM-HLEM geophysical approach to borehole siting in deeply weathered granitic terrains. *Groundwater*, *39*(4), 554–567. https://doi.org/10.1111/j.1745-6584.2001.tb02344.x

Ofterdinger, U., MacDonald, A. M., Comte, J.-C., & Young, M. E. (2019). Groundwater in fractured bedrock environments: Managing catchment and subsurface resources—An introduction. *Geological Society, London, Special Publications*, *479*, 1.1–1.9. https://doi.org/10.1144/SP479-2018-170

Perrin, J., Ahmed, S., & Hunkeler, D. (2011). The effects of geological heterogeneities and piezometric fluctuations on groundwater flow and chemistry in a hard-rock aquifer, southern India. *Hydrogeology Journal*, *19*(6), 1189–1201. https://doi.org/10.1007/s10040-011-0745-y

Pianosi, F., Beven, K., Freer, J., Hall, J. W., Rougier, J., Stephenson, D. B., & Wagener, T. (2016). Sensitivity analysis of environmental models: A systematic review with practical workflow. *Environmental Modelling & Software*, *79*, 214–232. https://doi.org/10.1016/j.envsoft.2016.02.008

Pianosi, F., Sarrazin, F., & Wagener, T. (2015). A Matlab toolbox for global sensitivity analysis. *Environmental Modelling & Software*, *70*, 80–85. https://doi.org/10.1016/j.envsoft.2015.04.009

Pianosi, F., & Wagener, T. (2015). A simple and efficient method for global sensitivity analysis based on cumulative distribution functions. *Environmental Modelling & Software*, *67*, 1–11. https://doi.org/10.1016/j.envsoft.2015.01.004

Pianosi, F., & Wagener, T. (2016). Understanding the time-varying importance of different uncertainty sources in hydrological modelling using global sensitivity analysis. *Hydrological Processes*, *30*, 3991–4003. https://doi.org/10.1002/hyp.10968

Pianosi, F., & Wagener, T. (2018). Distribution-based sensitivity analysis from a generic input-output sample. *Environmental Modelling & Software*, *108*, 197–207. https://doi.org/10.1016/j.envsoft.2018.07.019

Razack, M., & Lasm, T. (2006). Geostatistical estimation of the transmissivity in a highly fractured metamorphic and crystalline aquifer (Man-Danane Region, Western Ivory Coast). *Journal of Hydrology*, *325*(1–4), 164–178. https://doi.org/10.1016/j.jhydrol.2005.10.014

Renard, P., & De Marsily, G. (1997). Calculating equivalent permeability: A review. *Advances in Water Resources*, *20*(5–6), 253–278. https://doi.org/10.1016/S0309-1708(96)00050-4

Saltelli, A., Ratto, M., Andres, T., Campolongo, F., Cariboni, J., Gatelli, D., et al. (2008). *Global sensitivity analysis: The primer*. Hoboken, New Jersey: John Wiley & Sons.

Schmitter, P., Kibret, K. S., Lefore, N., & Barron, J. (2018). Suitability mapping framework for solar photovoltaic pumps for smallholder farmers in sub-Saharan Africa. *Applied Geography*, *94*, 41–57. https://doi.org/10.1016/j.apgeog.2018.02.008

Shishaye, H. A., Tait, D. R., Befus, K. M., & Maher, D. T. (2019). An integrated approach for aquifer characterization and groundwater productivity evaluation in the Lake Haramaya watershed, Ethiopia. *Hydrogeology Journal*, *27*, 2121–2136. https://doi.org/10.1007/s10040-019-01956-7

Taylor, R., & Howard, K. (2000). A tectono-geomorphic model of the hydrogeology of deeply weathered crystalline rock: Evidence from Uganda. *Hydrogeology Journal*, *8*(3), 279–294. https://doi.org/10.1007/s100400000069

Taylor, R., Tindimugaya, C., Barker, J., Macdonald, D., & Kulabako, R. (2010). Convergent radial tracing of viral and solute transport in gneiss saprolite. *Ground Water*, *48*(2), 284–294. https://doi.org/10.1111/j.1745-6584.2008.00547.x

Taylor, R. G., Scanlon, B., Döll, P., Rodell, M., van Beek, R., Wada, Y., et al. (2013). Ground water and climate change. *Nature Climate Change*, *3*, 322–329. https://doi.org/10.1038/nclimate1744

Thomson, P., Bradley, D., Katilu, A., Katuva, J., Lanzoni, M., Koehler, J., & Hope, R. (2019). Rainfall and groundwater use in rural Kenya. *Science of the Total Environment*, *649*, 722–730. https://doi.org/10.1016/j.scitotenv.2018.08.330

Velis, M., Conti, K. I., & Biermann, F. (2017). Groundwater and human development: Synergies and trade-offs within the context of the sustainable development goals. *Sustainability Science*, *12*, 1007–1017. https://doi.org/10.1007/s11625-017-0490-9

Wazed, M. S., Hughes, B. R., O'Connor, D., & Kaiser Calautit, J. (2018). A review of sustainable solar irrigation systems for sub-Saharan Africa. *Renewable and Sustainable Energy Reviews*, *81*, 1206–1225. https://doi.org/10.1016/j.rser.2017.08.039

WHO/UNICEF. (2020). The WHO/UNICEF JMP global database. Retrieved April 3, 2020, from https://washdata.org/data/household#!/

Wright, E. P. (1992). The hydrogeology of crystalline basement aquifers in Africa. *Geological Society, London, Special Publications*, *66*(1), 1–27. https://doi.org/10.1144/GSL.SP.1992.066.01.01

Zadeh, K. F., Nossent, J., Sarrazin, F., Pianosi, F., van Griensven, A., Wagener, T., & Bauwens, W. (2017). Comparison of variance-based and moment-independent global sensitivity analysis approaches by application to the SWAT model. *Environmental Modelling & Software*, *91*, 210–222. https://doi.org/10.1016/j.envsoft.2017.02.001